Fully adaptive propagation of the quantum-classical Liouville equation

Illia Horenko[a]
Freie Universitt Berlin, Arnimallee 2, D-14195 Berlin, Germany

Martin Weiser
Zuse Institute Berlin, Takustr. 7, D-14195 Berlin, Germany

Burkhard Schmidt and Christof Schütte
Freie Universitt Berlin, Arnimallee 2, D-14195 Berlin, Germany

In mixed quantum-classical molecular dynamics few but important degrees of freedom of a dynamical system are modeled quantum-mechanically while the remaining ones are treated within the classical approximation. Rothe methods established in the theory of partial differential equations are used to control both temporal and spatial discretization errors on grounds of a global tolerance criterion. The TRAIL (trapezoidal rule for adaptive integration of Liouville dynamics) scheme [I. Horenko and M. Weiser, J. Comput. Chem. **24**, 1921 (2003)] has been extended to account for nonadiabatic effects in molecular dynamics described by the quantum-classical Liouville equation. In the context of particle methods, the quality of the spatial approximation of the phase-space distributions is maximized while the numerical condition of the least-squares problem for the parameters of particles is minimized. The resulting dynamical scheme is based on a simultaneous propagation of moving particles (Gaussian and Dirac deltalike trajectories) in phase space employing a fully adaptive strategy to upgrade Dirac to Gaussian particles and, vice versa, downgrading Gaussians to Dirac-type trajectories. This allows for the combination of Monte-Carlo-based strategies for the sampling of densities and coherences in multidimensional problems with deterministic treatment of nonadiabatic effects. Numerical examples demonstrate the application of the method to spin-boson systems in different dimensionality. Nonadiabatic effects occurring at conical intersections are treated in the diabatic representation. By decreasing the global tolerance, the numerical solution obtained from the TRAIL scheme are shown to converge towards exact results. © *2004 American Institute of Physics.* [DOI: 10.1063/1.1691015]

I. INTRODUCTION

Quantum-classical models in molecular dynamics treat only few important degrees of freedom quantum-mechanically, while the remaining ones are approximated as classical many-body systems. In this way *nonadiabatic effects*, which are known to be of great importance for the correct description of many photochemical, photophysical, and biochemical applications, can be accounted for.[1–3] For the case of interaction between heavy (classical) and light (quantum) particles, such models have been mathematically justified by the *partial Wigner-transform* technique[4] in the context of the quantum-classical Liouville equation (QCLE).[5–10] The main advantage of such an approach is the mathematically *consistent coupling* of few decisive quantum degrees of freedom with the remaining classical ones.

In order to solve this equation for a realistic problem, one should apply a numerical method that can handle *multidimensional dynamics*. Such numerical approaches are based on the application of *sparse grids*[11,12] or on *particle methods*.[13,14] In contrast to frequently used conventional grid methods, they both scale reasonably well for medium dimensional problems. Sparse grids work best for smooth anisotropic densities with the grid being *aligned* to the propagated objects. In the context of molecular dynamics this grid alignment can be violated which drastically decreases efficiency. In the context of *particle methods*, the molecular system under consideration is represented as an ensemble of localized, moving basis functions, e.g., Dirac or Gaussian trajectories. *Particle methods* are especially convenient in this respect because: (1) they represent multidimensional objects *statistically* by ensembles of particles, (2) the spatio-temporal *dynamics* of these objects can be described by a collective motion of an ensemble of particles. Particle methods are especially useful for the simulation of *almost adiabatic* processes, where the molecular system is evolving adiabatically most of the time except for rare nonadiabatic transitions in the form of *stochastic hops* which are localized in time and space. Previous applications tackle either the time-dependent Schrödinger equation directly,[15–18] or hybrid quantum-classical models, such as quantum-classical molecular dynamics (QCMD).[19–27]

The simplest class of particle approaches for *nonadiabatic molecular dynamics* was first proposed by Tully: the empirically based *surface-hopping trajectory technique (SHT)* in which the propagated objects are modeled by an ensemble of classical Dirac-type trajectories.[28–30] In the course of the dynamical simulation, the particles may un-

[a]Author to whom correspondence should be addressed. Electronic mail: horenko@math.fu-berlin.de

dergo "hops" between different eigenstates of the quantum subsystem in order to model nonadiabatic transitions in a stochastic manner. Many applications of this method are reported in the field of molecular dynamics, even for very large systems, e.g., vibronic processes[31,32] or reactions in enzymes.[19,33–36]

Particle methods based on a superposition of Gaussian wave packets for *adiabatic quantum dynamics* as first introduced by Heller[16,37–40] have become popular and inspired a variety of methods for the description of *nonadiabatic effects*, e.g., the multiple spawning method[41–43] and the multithreads method.[44–46] Quite often, the proposed algorithms rely on two simplifying assumptions: (1) the independent particle approximation (IPA, also known as IGA—independent Gaussians approximation), which assumes that the particles can be propagated independently, and (2) the locally harmonic approximation (LHA), which assumes that the "width" of each particle is smaller than the length over which the potential deviates significantly from a quadratic shape. Note that Dirac function representations as commonly realized in classical molecular dynamics codes propagate trajectories independently and so far rely on the IPA assumption. Both assumptions are sufficiently valid in a number of practically relevant situations for short simulation times.

There are, however, several situations where neither IPA nor LHA are valid, e.g., nonadiabatic effects and reduced models violate the IPA, whereas the LHA is in general violated for realistic potentials and propagation times. This motivated the development of algorithms which do not depend on these assumptions. The strategy proposed by Walkup *et al.*[47] and Prezhdo *et al.*[48] employs higher-order derivatives of the potential for propagating the distribution function. However, in the case of realistic multidimensional applications the problem of calculating these derivatives becomes intractable. Alternatively, Sawada *et al.* suggested a least squares particle approximation of the underlying dynamics in terms of the minimum error method (MEM).[17] These concepts were further developed resulting in *multiconfigurational Gaussian methods*.[49–51] A similar concept was also proposed by Billing,[52,53] where products of a Gaussian and orthogonal polynomials, e.g., eigenfunctions of a harmonic oscillator, were used for the space discretization of the PDE in a moving grid fashion. Heuristic strategies for adapting the number of particles based on monitoring eigenvalues of the overlap matrix were described in the literature,[17,18,41–43] but are not numerically justified. In all those approaches there is no possibility to control the spatial approximation error during the integration which can have two consequences: First, the equations of motion can become ill-conditioned and hence intractable in the course of the propagation. Second, the number and position of particles needed for a reliable representation of solution is changing in time.

All of the existing particle methods can be divided into two groups depending on the discretization scheme for partial differential equation (Schrödinger, QCLE, etc.).[54] The first group is known under the name *methods of lines* and all of the above-mentioned approaches belong to that class. The common idea is that equations of motion are derived in the form of a system of ordinary differential equations (ODEs)

by, e.g., a least squares approximation to the continuous evolution given by the partial differential equation (PDE). The resulting ODEs can then be solved best with the help of *explicit symplectic* ODE-integrators which allow stable propagation for long simulation times. However, the method of lines is hampered by a crucial shortcoming: It does not allow to control the space-discretization error once the spatial particle discretization has been fixed at the initial time step.

This problem is circumvented in the second group of numerical methods for dynamical PDEs, also known as *Rothe methods*. It presumes a primal time-discretization of the PDE followed by a solution of stationary PDEs at each time step. This concept provides a possibility of controlling both space- and time-discretization errors and allows for a *fully adaptive integration* of the respective dynamics. In the context of adiabatic molecular dynamics this was first achieved in the TRAIL method (trapezoidal rule for adaptive integration of Liouville dynamics).[55] In the current paper we present an extension of the TRAIL-framework to the numerical solution of the quantum-classical Liouville equation thus allowing to include nonadiabatic effects.

In most molecular dynamics simulations, an adiabatic representation of the electronic problem is chosen. However, the presence of *conical intersections* induces numerical problems in particle methods due to the singularity in the nonadiabatic coupling. In contrast, the diabatic coupling is not localized in time and space. Hence, diabatic propagations are numerically more demanding and are not particularly amenable for the surface-hopping schemes. Although most quantum chemical methods provide PESs and couplings in adiabatic representation, there are ways of diabatization recently presented in the literature.[56,57]

The remainder of the paper is organized as follows: Section I is devoted to the description of the QCLE model and the comparison of different representations from a numerical point of view. In Sec. II, the principles of the TRAIL-method and its application to QCLE are discussed. Finally, Sec. III contains numerical examples, describing the application of the method to prototypical model systems.

II. QUANTUM-CLASSICAL LIOUVILLE EQUATION

Consider a bi-component physical or chemical quantum system composed of a heavy particle with mass M, position $\hat{R}$, momentum $\hat{P}$, and a light particle characterized by m, $\hat{r}$, $\hat{p}$. Typically, in molecular problems, heavy and light particles are nuclei and electrons, respectively. Alternatively, they can be also interpreted as slow and fast nuclear degrees of freedom, e.g., in the case of proton transfer processes.[33,58,59] The corresponding Hamiltonian contains an interaction potential $\hat{U}$ as well as kinetic energy associated with the two particles

$$\hat{H}(\hat{r},\hat{R},\hat{p},\hat{P}) = \hat{U}(\hat{r},\hat{R}) + \frac{1}{2m}\hat{p}^2 + \frac{1}{2M}\hat{P}^2, \qquad (1)$$

where generalization to the case of several heavy and/or several light particles and/or to the use of non-Cartesian coordi-

nates is straightforward. Casting this Hamiltonian into coordinate representation and adopting the scaling procedure introduced in earlier work[20] results in

$$\hat{H}(\hat{r},\hat{R},-i\nabla_r,-i\epsilon\nabla_R)=U(r,R)+\frac{1}{2}\Delta_r+\frac{\epsilon^2}{2}\Delta_R, \qquad (2)$$

where the dimensionless smallness parameter

$$\epsilon=\sqrt{\frac{m}{M}}\ll 1 \qquad (3)$$

shall be used throughout the rest of this work to indicate the deviation from adiabatic behavior.

The diabatic representation of the total Hamiltonian is obtained by using an orthonormal, complete basis set to represent the light-particle states

$$H_d(R,\nabla_R)=V(R)-\frac{\epsilon^2}{2}\Delta_R, \qquad (4)$$

where $V(R)$ stands for a matrix representation of the light-particle Hamiltonian, i.e., the first two terms on the r.h.s. of Eq. (2). Alternatively, an adiabatic representation is obtained by diagonalizing $V(R)$ yielding the following expression for the Hamiltonian:

$$H_a(R,\nabla_R)=E(R)-\frac{\epsilon^2}{2}(\Delta_R+2C(R)\cdot\nabla_R+T(R)), \qquad (5)$$

where the eigenvalues $E(R)$ are the adiabatic potential energy (hyper-)surfaces and where nonadiabatic coupling is due to the parametric R-dependence of the adiabatic light-particle states $|\phi_i(R)\rangle$. In particular, the matrix elements of the first and second order nonadiabaticity operators are given by

$$C_{ij}(R)=\langle\phi_i(R)|\nabla_R|\phi_j(R)\rangle,$$
$$T_{ij}(R)=\langle\phi_i(R)|\Delta_R|\phi_j(R)\rangle, \qquad (6)$$

where the first tensor is anti-Hermitian while no symmetry relation holds for the second one. Note, that both in the diabatic (4) and adiabatic case (5), the expansion in terms of light-particle states results in matrix valued operators acting on the heavy-particle degrees of freedom. The density operator $\hat{\rho}$ can be treated in an analogous way.[60] We restrict ourselves to the treatment of pure states, but generalization to mixed states is possible.[8,61]

The full quantum dynamics is governed by the Liouville–von Neumann equation

$$\partial_t\hat{\rho}(t)=-\frac{i}{\epsilon}[\hat{H},\hat{\rho}(t)]. \qquad (7)$$

For a one-component system it is well known that the classical Liouville equation can be derived as the $\hbar\to0$ limit of the quantum Liouville equation by means of the Wigner transform.[4,62] In close analogy, a partial Wigner transform for a bi-component system can be defined which acts only on the heavy-particle degrees of freedom while leaving the light-particle dynamics unchanged.[6] Application to the quantum Liouville equation (7) readily yields the *Quantum-Classical Liouville Equation* (QCLE),

$$\partial_t\rho_W=-\frac{i}{\epsilon}((H\rho)_W-(\rho H)_W)$$

$$=-\frac{i}{\epsilon}[H_W,\rho_W]_- -\frac{1}{2}(\{H_W,\rho_W\}-\{\rho_W,H_W\})+\mathcal{O}(\epsilon), \qquad (8)$$

where all higher-order terms in the expansion of the Wigner transform of a commutator have been neglected.[62] The structure of the equation already suggests the existence of a purely quantum-mechanical (commutator) evolution as well as classical or quantum-classical connected with the Poisson brackets which are defined in the usual way, $\{A,B\}=\nabla_P A\cdot\nabla_R B-\nabla_R A\cdot\nabla_P B$. Inserting the diabatic representation (4) into (8), we obtain the *diabatic QCLE* for the dynamics of the Wigner-transformed density matrix $X_d=\rho_W$,

$$\partial_t X_d(R,P,t)=-\frac{i}{\epsilon}[V(R),X_d(R,P,t)]_- -P\cdot\nabla_R X_d(R,P,t)$$

$$+\tfrac{1}{2}[\nabla_R V(R),\nabla_P X_d(R,P,t)]_+ +\mathcal{O}(\epsilon). \qquad (9)$$

Alternatively, by inserting Eq. (5) into Eq. (8) the *adiabatic QCLE* is derived

$$\partial_t X_a(R,P,t)=-\frac{i}{\epsilon}[E(R)-i\epsilon P\cdot C(R),X_a(R,P,t)]_-$$

$$+\tfrac{1}{2}[E(R),[C(R),\nabla_P X_a(R,P,t)]_+]_-$$

$$-P\cdot\nabla_R X_a(R,P,t)$$

$$+\tfrac{1}{2}[\nabla_R E(R),\nabla_P X_a(R,P,t)]_+ +\mathcal{O}(\epsilon). \qquad (10)$$

As discussed in detail in other work,[5,60] the first term on the r.h.s. describes the purely quantum mechanical evolution giving rise to phase oscillations of the coherences [off-diagonal elements of density matrix, $X(R,P)$] only. In contrast, the last two terms describe purely classical evolution of the densities and coherences along the adiabatic potential energy surfaces or arithmetic means there of respectively. The remaining two terms involving the coupling function, $C(R)$, are of genuinely quantum-classical nature and describe the nonadiabatic exchange of densities and coherences. Using existing particle methods, e.g., stochastically surface hopping trajectories[28] or Gaussian packets,[60] the adiabatic formulation of the QCLE is more amenable to numerical solution than the diabatic one. This is because typically the nonadiabatic coupling, $C(R)$, is large only for a limited part of coordinate space, i.e., near avoided intersections while non-adiabatic effects may become negligible outside these regions.

In the present work, however, the quantum-classical dynamics in the presence of conical intersections is to be investigated. A consistent numerical treatment using the adiabatic formulation is not possible because of singularities of the nonadiabatic coupling, $C(R)$, as well as discontinuities of the classical forces, $-\nabla E(R)$, at the intersections. Hence, there is a strong motivation for developing efficient and accurate integrators for the diabatic QCLE (9). In particular, the (typically nonlocalized) coupling through the off-

diagonal elements of $V(R)$ are expected to render the evolution strongly nonclassical. Consequently, there is a need for development of adaptive methods which can dynamically create or annihilate particles according to preset accuracy criteria.

III. APPLICATION OF THE TRAIL-SCHEME TO QCLE

A number of approaches can be applied in order to integrate the QCLE. The standard *method of lines* particle strategy implies some initial space discretization of such an equation in terms of some basis functions, such as Dirac trajectories[10] (frozen) Gaussian particles[41–43,60,63] or frozen Gaussian multiplied with some orthogonal polynomials.[53] This produces a system of ordinary differential equations for the parameters of basis functions (such as amplitudes, centers, etc.) which can be integrated with the help of standard ODE tools for a long propagation times. A major drawback of such a methodology is that the quality of a space-discretization and the exactness of the expectation values calculated remains uncontrolled. In order to construct a fully adaptive method we follow another strategy and employ the *Rothe method*[64] of *implicit* semidiscretization in time. This leaves us with a stationary PDE to be solved in each time step and allows for the control of the global error, which consists of space and time discretization errors.

A. Adaptive time discretization

Let us denote the operator in the r.h.s. of Eq. (9) or (10) as $\mathcal{L}$. In order to select a proper time discretization scheme one should take into account the two following facts: (1) The predominantly imaginary spectrum of the QCLE operator $\mathcal{L}$ will cause instability using explicit time-discretization schemes. (2) Evaluation of the QCLE operator can become expensive for multidimensional problems (each evaluation of $\mathcal{L}$ will mean a solution of the multidimensional variation problem connected with the electronic structure calculation). That is why we consider here the simplest implicit scheme demanding only one evaluation of the operator $\mathcal{L}$ for a given X per time step, the well-known trapezoidal rule

$$\left(I - \frac{\tau}{2}\mathcal{L}\right)\bar{X}(t+\tau) = \left(I + \frac{\tau}{2}\mathcal{L}\right)X(t), \qquad (11)$$

where $\bar{X}$ is the value obtained by the discrete evolution, starting from the (exactly available) initial value X and where I denotes the identity operator. Moreover, the trapezoidal integrator conserves first integrals, which implies conservation of volume and energy for the QCLE setting.

For adaptivity in time we need three essential ingredients: an error estimator, a step size selection scheme, and a desired tolerance. We briefly recollect this ingredients of the TRAIL-scheme (cf. Ref. 55).

1. Error estimator

Denoting the exact evolution of Eq. (9) or (10) by Φ, we estimate the unknown error

$$\epsilon_t := \|\bar{X}(t+\tau) - \Phi_\tau X(t)\| \qquad (12)$$

by the difference between the trapezoidal rule and some easily computable comparison propagator $\hat{\Psi}_\tau$ of lower order, e.g., the explicit Euler method,

$$[\bar{\epsilon}_t] := \|\bar{X}(t+\tau) - \hat{\Psi}_\tau X(t)\|. \qquad (13)$$

The step is accepted if $[\bar{\epsilon}_t]$ is sufficiently small, i.e., $[\bar{\epsilon}_t] \leq \text{TOL}_t$, where TOL_t is a user-prescribed accuracy requirement. Otherwise we reduce the step size and repeat the step. Note that $[\bar{\epsilon}_t]$ necessarily estimates the error $\hat{\epsilon}_t$ of the less accurate comparison propagator $\hat{\Psi}_\tau$ instead of the computationally unavailable error of the trapezoidal rule.

A tempting idea would be to choose $\hat{\Psi}_\tau$ from efficient explicit particle propagators, which have been developed under the LHA and IPA assumptions for locally harmonic potentials.[37,60] However, in the case of strongly nonharmonic potentials and GPPs with nonvanishing width, these propagators are of order zero and do not represent the dynamics adequately. Although being a reasonable approximation to the exact evolution Φ_τ, such propagators provide worse error estimates than the explicit Euler scheme.

2. Step size selection scheme

We assume the comparison propagator $\hat{\Psi}_t$ is of order one, such that

$$\hat{\epsilon}_t \doteq C\tau^2 \qquad (14)$$

holds locally for some slowly varying constant C. Substituting $[\bar{\epsilon}_t]$ for ϵ_t and aiming at an error of σTOL_t with some safety factor $\sigma < 1$, we obtain an optimal step size

$$\tau_{\text{opt}} = \sqrt{\frac{\sigma\text{TOL}_t}{[\bar{\epsilon}_t]}}\,\tau, \qquad (15)$$

which is used for the next step or recomputing the current time step, respectively.[54]

B. Adaptive phase-space discretization

Consider arbitrary *particles* $g(\bar{R}_n^{i,j}(t), \bar{P}_n^{i,j}(t), \bar{G}_n^{i,j}(t))$ in phase space. We will distinguish between *particles* (being some smooth moving basis functions) and *sample points* (Dirac delta-trajectories). For approximating the (i,j) element of matrix X to be propagated, we use a linear combination of such particles g,

$$X^{i,j}(t) = \sum_{n=1}^{N^{i,j}} y_n^{i,j}(t) g(\bar{R}_n^{i,j}(t), \bar{P}_n^{i,j}(t), \bar{G}_n^{i,j}(t)) \qquad (16)$$

centered at $(\bar{R}_n^{i,j}, \bar{P}_n^{i,j})(t)$ in phase space, scaled by the amplitudes $y_n^{i,j}(t)$ being real-valued functions for $i = j$ (densities) and complex-valued for $i \neq j$ (coherences). Additionally, the shape of the particles is allowed to depend on a set of shape parameters $\bar{G}_n^{i,j}(t)$.

The *Rothe method* for propagation of the partially Wigner transformed density X by the implicit trapezoidal rule (11) leads to a stationary PDE-problem to be solved in each time step. Spatial dicretization of this PDE turns Eq. (11) into the approximation problem of finding a new density $\bar{X}(t+\tau)$ representable by particles such that

$$\epsilon_x = \left\| \left(I - \frac{\tau}{2} \mathcal{L} \right) \bar{X}(t+\tau) - \left(I + \frac{\tau}{2} \mathcal{L} \right) X(t) \right\|_{\mathcal{L}_2} \leqslant \mathrm{TOL}_x. \quad (17)$$

Here, TOL_x is a tolerance which now has to be matched with the user-prescribed accuracy requirement TOL_t—for details see below. By introducing K_N test points $(R_n^{i,j}, P_n^{i,j})$, we reduce Eq. (17) to a computationally tractable approximation problem

$$[\epsilon_x] = \left\| \left(I - \frac{\tau}{2} \mathcal{L} \right) X(t+\tau) - \left(I + \frac{\tau}{2} \mathcal{L} \right) X(t) \right\|_{\{R_i, P_i\}} \leqslant \mathrm{TOL}_x, \quad (18)$$

where $\| \cdot \|_{\{R_i, P_i\}}$ denotes the discretized $\mathcal{L}_2$-norm taken at the test points $\{R_i, P_i\}$. In view of computational efficiency we aim at a representation with a minimal number of particles, and hence derive the particles' parameters from the minimization problem $[\epsilon_x] \rightarrow \min$. Depending on which parameters in Eq. (16) are to be chosen [either only the amplitudes $A_n^{i,j}$, or both amplitudes and phase space positions $(\bar{R}_n^{i,j}, \bar{P}_n^{i,j})$ of the particles' centers], we arrive at a linear or nonlinear least squares problem. In the linear version, the system has K_N equations and $\#\mathrm{dof}(N) = N$ unknowns $A_n^{i,j}$ for the particles' amplitudes defining $X(t+\tau)$, and can be solved by a single QR decomposition of the influence matrix,[65]

$$\mathbf{A} = \frac{\partial}{\partial y} \left[\left(I - \frac{\tau}{2} \mathcal{L} \right) X(t+\tau) \right]. \quad (19)$$

In the nonlinear variant, the system has K_N equations and $\#\mathrm{dof}(N) = (1 + 2n_{\mathrm{dim}})N$ degrees of freedom $A_n^{i,j}$, $\bar{R}_n^{i,j}$, and $\bar{P}_n^{i,j}$ defining $X(t+\tau)$. Due to the better approximation capability offered by also adjusting the particles' centers, the number of particles necessary to satisfy the accuracy requirement (18) can be expected to be considerably smaller than for the linear approach. However, this does not necessarily translate into fewer degrees of freedom, or fewer sample points. For solving the nonlinear least squares problem, a Gauss–Newton method should be used, which may require multiple QR decompositions of the influence matrix

$$\mathcal{A} = \frac{\partial}{\partial(y, \bar{R}, \bar{P})} \left[\left(I - \frac{\tau}{2} \mathcal{L} \right) X(t+\tau) \right]. \quad (20)$$

Whether this is compensated by the better approximation capability is not clear *a priori*.

There are several possibilities to choose the particle collection used to represent $X(t+\tau)$ in the beginning of the time step. Selecting particles in unsuitable regions of the phase space will prevent the linear least squares approach from meeting the accuracy requirement (18), thus triggering the discretization refinement developed below. For the nonlinear least squares approach, it will increase the number of Gauss–Newton steps and hence decrease the computational efficiency. A sufficiently good initial guess for the solution of the least squares problem is therefore necessary for computational efficiency in both variants.

Another question which has to be addressed is the choice of sample points (R_i, P_i), $i = 1,...,K_N$. For the least squares problem (18) not to be underdetermined, we require at least

$K_N \geqslant \#\mathrm{dof}(N)$ sample points, preferably distributed in accordance with the quasiprobability density $X(t)$. K_N should be significantly larger than $\#\mathrm{dof}(N)$ in order to improve the robustness of the least squares approximation and to provide a local error estimator for spatial adaptivity (see below). Since performing a Monte Carlo sampling at every time step is prohibitively expensive, we suggest to select the sampling points according to the following scheme: For the first step at $t = 0$ we take the sample points from the initial particle approximation. For subsequent steps, we suggest to take again the centers of the particles i.e., $(R_i(t+\tau), P_i(t+\tau))$ $= (\bar{R}_i(t+\tau), \bar{P}_i(t+\tau))$, $i = 1,...,N$, and additionally the remaining sampling points from the previous step propagated independently of each other in time along classical trajectories, i.e., $(R_i(t+\tau), P_i(t+\tau)) = \Phi_\tau(R_i(t), P_i(t))$, $i = N + 1,...,K_N$. This implies two types of basis functions, namely Dirac trajectories and smooth particles being propagate simultaneously.

It may happen that the number N of particles chosen to fit the initial state $X(0)$ becomes inadequate during the propagation, for three different reasons: (a) A more complicated distribution $X(t)$ turns up later in time, such that more particles are needed to represent the distribution $\bar{X}(t)$ with the required accuracy. (b) Two or more particles can come close to each other, such that the least squares problem (18) becomes ill-conditioned. (c) The distribution may develop a simpler structure, such that it is advisable to reduce the number of particles for computational efficiency. The first situation requires the upgrade of new smooth particles from Dirac trajectories, whereas the latter ones require the downgrading of particles to trajectories.

Let us first consider the case that the number of particles is too small, such that the accuracy requirement (18) cannot be satisfied. In this case, as few as possible additional particles have to be created in order to reduce the approximation error sufficiently. Fortunately, the local residuals

$$\epsilon_k = \left\| \left(I - \frac{\tau}{2} \mathcal{L} \right) X(R_k, P_k, t+\tau) - \left(I + \frac{\tau}{2} \mathcal{L} \right) X(R_k, P_k, t) \right\| \quad (21)$$

provide a useful local error indicator suitable for extending the particle set. A similar error indicator has been proposed by Iske and Levesley[66] in the context of scattered data approximation. The following scheme is intended to insert the new particles at positions in phase-space, where the approximation error is largest, and hence to improve the approximation at a small cost.

Assume the sample points $(R_k^{i,j}, P_k^{i,j})$ (which are not also centers of existing particles) with corresponding *statistical weights* $\omega_k^{i,j}$, $k = N+1,...,K_N$, are sorted descendingly by their local residual $\omega_k^{i,j} \epsilon_k$. Let $j > N$ be minimal such that

$$\sum_{k=j+1}^{K_N} \omega_k^{i,j} \epsilon_k \leqslant \mathrm{TOL}_x \quad (22)$$

holds, or $j = K_N$ if Eq. (22) cannot be satisfied. We then suggest to upgrade the sample points $N+1,...,j$ to particles with centers $(R_k^{i,j}, P_k^{i,j})$, $k = N+1,...,j$, amplitude zero, and shape matrix λI, and create at least $2n_{\dim}(K_N - j)$ new sample points in the vicinity of the newly created particles by some Monte Carlo method. N and K_N should be increased accordingly to j and $K_N + 2n_{\dim}(K_N - j)$, respectively.

With the enlarged particle set at hand, the least squares problem is solved again in order to meet the requirement (18). If necessary, the adaptive refinement is repeated until finally (18) is met.

Related greedy algorithms for spatial adaptivity in different contexts have been proposed by Schaback *et al.*[67,68]

Let us now turn to the case that the least squares problem (18) becomes ill-conditioned due to similarly shaped particles being too close to each other. Sawada *et al.*[17] suggest to drop an arbitrary Gaussian and do a refitting of the remaining ones whenever one eigenvalue of the overlap matrix becomes small. While this criterion is reported to work, neither does it take the approximation error into account nor does it indicate which Gaussian to drop or how small an eigenvalue must become. Wan *et al.*[44] suggest removing Gaussians with an amplitude below 10^{-12} and to collapse any two Gaussians which are too close to each other. While this can indeed cure the numerical stability problems, no indication is given about how close two Gaussians must be or how the cutoff value of the amplitude was chosen.

As a pruning method oriented at the numerical stability and the approximation error, we propose to use a column permutation strategy[69] for the QR decomposition together with a numerical rank decision based on the subcondition number[65] in order to identify and remove exactly those columns and downgrade their associated particles which make Eq. (18) numerically singular to sample points. Moreover, a careful examination of the least squares residual enables the identification of even more particles which are not necessary to obtain the requested accuracy, and thus can be removed. Pruning of the particles collection should be realized by downgrading unnecessary particles to sample points.

To be more precise, in the linear least squares setting, assume the columns of A and correspondingly the rows of x of the linear least squares problem $\|Ax - b\| = \min$ have been sorted such that for the QR decomposition $A = Q\mathcal{R}$ the relations

$$|\mathcal{R}_{ii}| \geqslant |\mathcal{R}_{i+1,i+1}| \quad \text{for } i = 1,...,\#\text{dof}(N) - 1$$

hold. Construct a partition

$$\mathcal{R} = \begin{pmatrix} \mathcal{R}_1 & S_1 & S_2 \\ & \mathcal{R}_2 & S_3 \\ & & \mathcal{R}_3 \\ & & 0 \end{pmatrix}, \quad x = \begin{pmatrix} x_1 \\ x_2 \\ x_3 \end{pmatrix}, \quad Q^T b = \begin{pmatrix} b_1 \\ b_2 \\ b_3 \\ b_4 \end{pmatrix}, \tag{23}$$

such that the following conditions are satisfied:

$$\max_i |(\mathcal{R}_3)_{ii}| \leqslant \frac{1}{\kappa}|(\mathcal{R}_1)_{11}|$$

$$< \min_i |(\mathcal{R}_2)_{ii}| \sqrt{\|b_2\|^2 + \|b_3\|^2 + \|b_4\|^2} \leqslant \sigma\text{TOL}_x$$

for κ being the maximal accepted least squares condition (somewhere around $\kappa = 10^8$) and $0 < \sigma < 1$ some safety factor which can be adjusted to balance pruning and spawning. A default value of $\sigma = 0.9$ is suggested. Note that $\|b_4\|$ is the smallest possible approximation error that can be achieved at all with the present collection of particles, and similarly $\sqrt{\|b_3\|^2 + \|b_4\|^2}$ is the minimal error that can be obtained in a numerically stable way.

The columns of A and the particles corresponding to the degrees of freedom in x_3 can be removed on the observation that they are numerically linearly dependent on the columns corresponding to x_1 and x_2, and hence are redundant.

Furthermore, the degrees of freedom in x_2 contribute least to the approximation capability of the remaining particle collection. Sacrificing some accuracy while still satisfying the accuracy requirement (18) allows us to improve the computational efficiency.

In case no such partition can be found, i.e., $\sigma\text{TOL}_x < \sqrt{\|b_3\|^2 + \|b_4\|^2} \leqslant \text{TOL}_x$, just the numerically linearly dependent degrees of freedom are cancelled. If the accuracy requirement (18) cannot be fulfilled at all, i.e., $\sqrt{\|b_3\|^2 + \|b_4\|^2} > \text{TOL}_x$, the spawning procedure described above has to be performed.

In the setting of the nonlinear least squares fitting, the correspondence of columns in A to particles is no longer one to one, such that the pruning procedure described above has to be modified. Numerical stability even in the case of linearly dependent columns can be maintained by setting $x_3 = 0$ without removing the corresponding degrees of freedom. We suggest performing the last Gauss–Newton step, when the particles' centers are already close to the solution, in a reduced fashion by fitting only the amplitudes. In this way, the pruning scheme developed for the linear least squares case can be transferred to the nonlinear case as well.

Unfortunately, the time error estimator $[\bar{\epsilon}_t] = \|\bar{X}(t+\tau) - \hat{\Psi}_\tau X(t)\|$ is still computationally unavailable. Its canonical substitute $[\epsilon_t] := \|X(t+\tau) - \hat{\Psi}_\tau X(t)\|_{\{R_i, P_i\}}$ depends on the spatial discretization error ϵ_x, which should not destroy the overall quality of the error estimate. In view of $[\bar{\epsilon}_t] \doteq C\tau^2$ and $\epsilon_t \doteq C\tau^3$, and in order not to destroy the second order convergence of the trapezoidal rule, we aim at $\epsilon_x \doteq \epsilon_t$ and hence impose the accuracy matching $\text{TOL}_x = \tau\text{TOL}_t$.

C. Gaussian phase-space packets

We suggest to use Gaussian phase-space packets (GPPs) (Refs. 70, 71) as smooth particles in the TRAIL method,

$$g_n(R,P) = \exp\left[-\begin{pmatrix} R - R_n \\ P - P_n \end{pmatrix}^T \mathbf{G}_n \begin{pmatrix} R - R_n \\ P - P_n \end{pmatrix}\right], \tag{24}$$

where $\mathbf{G}_n$ is the real, symmetric, positively definite $2D \times 2D$ matrix defining the elliptic phase-space contour of GPP. The simplest choice of the starting point for the Gauss–Newton method is the current GPP collection $X(t)$. How-
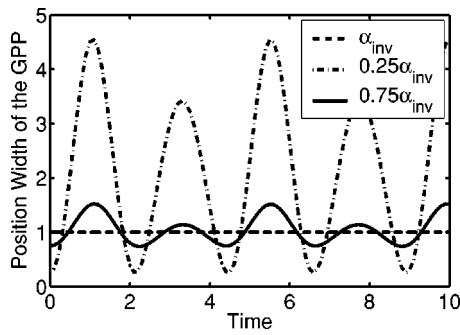
FIG. 1. Position uncertainties as functions of time for GPPs in anharmonic potential $V(R) = R^2 + 0.1R^3$. Narrow GPPs expand their position width much faster than GPPs of invariant position width α_{inv} from Eq. (29).

ever, the time step τ is limited by the requirement that the initial guess should be sufficiently good such that the local Gauss–Newton iteration converges quickly and reliably to the nearest local solution. Similarly, if only the amplitudes y_n are fitted by a linear least squares approach, a good initial guess yields a particle set which is well suited to represent the solution. Thus, the accuracy requirement (18) can be satisfied with fewer GPPs.

For these reasons, the employment of a cheaply computable predictor providing a better initial guess can be expected to improve the performance of the propagation considerably, by allowing larger time steps (in the Gauss–Newton case) and by decreasing the number of necessary GPPs (in the linear least squares case).

As a predictor for the QCLE considered here one on can use any kind of explicit surface-hopping algorithm or even a classical transport process of GPPs realized by the modified leapfrog propagator.[63] In the simple case of both LHA and IPA holding, the Gauss-particles in the ensemble can be propagated independently with evolution equations for the parameters R_n, P_n, and G_n of Eq. (16),

$$\partial_t \bar{R}_n = M^{-1} \bar{P}_n, \tag{25}$$

$$\partial_t \bar{P}_n = -\nabla_R V(\bar{R}_n), \tag{26}$$

$$\partial_t \bar{G}_n = C(\bar{R}_n)\bar{G}_n + \bar{G}_n C^T(\bar{R}_n), \tag{27}$$

where

$$C(\bar{R}_n) = \begin{pmatrix} 0 & V^{(2)}(\bar{R}_n) \\ -M^{-1} & 0 \end{pmatrix},$$

where $V^{(2)}(\bar{R}_n)$ denotes the Hesse-matrix of the potential V.

This scheme works well for low to medium dimensional problems, but requires the second derivative of the potential to be evaluated. This evaluation can become expensive for higher dimensional problems. Another problem is connected to the validity of LHA and IPA for anharmonic potentials. For sufficiently narrow GPPs, the LHA holds at least approximately even for nonharmonic potentials, such that the predictor solution can be expected to provide a good approximation of the classical part of the QCLE. It is desirable to choose the shape matrixes G_n in such a way that the position space width of GPPs does not exceed some threshold. As it can be seen from Fig. 1, even when the initial

GPPs are narrow in position space, they become increasingly wide and oscillate around the *fixed point* of Eq. (27) (which in the case of $\int X dR dP = 1$ describes the evolution of a squeezed state, i.e., a displaced quantum-mechanical ground state in phase-space[72]). This produces phase-space errors and can be avoided in the case when all shapes G_n of GPPs are selected as

$$G_{inv} = \begin{pmatrix} \alpha_{inv} & 0 \\ 0 & \gamma_{inv} \end{pmatrix} \tag{28}$$

and both α_{inv} and γ_{inv} are diagonal matrixes derived as solutions of the following system:

$$\alpha_{inv} = M^{-1} \langle V^{(2)} \rangle \gamma_{inv},$$

$$\sqrt{\det(\gamma_{inv}) \det(\alpha_{inv})} = \frac{\pi^d n}{\int X dR dP},$$

$$\{\gamma_{inv}\}_{i,i} = \gamma, \tag{29}$$

where n is a number of GPPs in the representation of X, d is a spatial dimension of the problem, γ is some positive real number, and $\langle V^{(2)} \rangle = \int X V^{(2)} dR$ is a mean Hesse matrix. The first of above equations gives the fix point solution of Eq. (27), whereas the second imposes a fixed volume of GPP being equal to $n^{-1} \int X dR dP$.

This allows us to apply the classically transported *frozen* GPPs as a predictor for QCLE integration, i.e., GPP's centers are propagated accordingly to Newtonian equations of motion while fixed shapes are chosen from Eq. (29). This strategy can represent only the adiabatic transport of densities. In such a case the nonadiabatic effects of the QCLE are reproduced by the corrector part of the TRAIL-method alone. This does not impair the quality of the solution, but may affect the efficiency of the algorithm.

D. Volume and energy conservation

An advantage of the trapezoidal rule is its property of conserving first integrals of linear dynamics exactly. This encloses conservation of volume and energy of the Wigner densities. In connection with a straightforward least-squares approximation as a spatial discretization of the quasidensities, however, this favorable property is lost for finite spatial tolerances, and only recovered in the limit $TOL_x \rightarrow 0$. Such a significant reduction of the spatial tolerance, however, increases the computational complexity substantially and is in general not feasible.

In view of the conservation property of the exact trapezoidal rule, the minimization of the approximation error may be constrained to the affine subspace of discretized quasidensities with exactly the same volume and energy,

$$\min \left\| \left(I - \frac{\tau}{2}\mathcal{L} \right) X(t+\tau) - \left(I + \frac{\tau}{2}\mathcal{L} \right) X(t) \right\|_{\{R_i, P_i\}} \tag{30}$$

subject to

$$V(X(t+\tau)) = V(X(t)) \tag{31}$$

and

$$E(X(t+\tau)) = E(X(t)). \tag{32}$$

An efficient and numerically stable algorithm for solving such equality constrained least squares problems results from a slight modification of the usual QR decomposition.[73] The restriction of the discretized quasidensities to the affine subspace of constant volume and energy is consistent with the time discretization and allows for exact conservation even for moderate spatial tolerances.

IV. NUMERICAL EXAMPLE

In this section we want to investigate the performance of the TRAIL approach for the numerical treatment of quantum-classical dynamics in a fully adaptive manner. The prototypical one- or higher-dimensional systems chosen here are characterized by crossings or conical intersections of potential energy surfaces, respectively, are known to play a key role in many photochemical processes.[1–3] Moreover, the strongly nonadiabatic dynamics encountered at the singularities necessitates a propagation of the QCLE (9) in the diabatic representation thus providing a much more demanding test for the numerical integration scheme. Finally, note that—except for the single crossing case—all systems studied here are spin boson systems, which are widely used as a simple model for open quantum systems. In a diabatic picture, they are described as linearly coupled harmonic oscillators. For these class of systems, the diabatic quantum-classical dynamics exactly coincides with fully quantum dynamics.[10] This facilitates a comparison of the TRAIL/QCLE results with numerically exact solutions of the Schrdinger equation using FFT methods.[74]

A. One-dimensional examples

1. Single crossing

As a first test for the QCLE-based implementation of the adaptive strategy we choose the *adiabatic* representation of the *single crossing* example described in Ref. 60. The propagated object $X(t)$ is a matrix-valued quasidistribution function (elements of the matrix can become negative or complex-valued). As it follows from the structure of the adiabatic QCLE, in the regions where the nonadiabatic coupling is small, the dynamics of diagonal elements of the matrix $X(t)$ is governed by a classical transport along the corresponding adiabatic surfaces. The nondiagonal elements acquire oscillations with a frequency depending on the energy gap between the surfaces. In the *crossing region* the nonadiabatic transitions can occur, transferring density between different diagonal elements of $X(t)$. Each of the density-matrix elements is represented as a linear combination of GPPs, which can be updated during the propagation according to the tolerance criterion as described above. As it can be seen from Fig. 2, the adaptive implicit integrator converges towards the exact solution with reduction of tolerance and reproducing correctly the weak Stueckelberg oscillation. In the crossing region the number of GPPs is growing due to the strong *nonadiabatic coupling* between the two adiabatic levels and geometric complexity of the densities and coherences in this region. After the passage through the crossing region GPPs are dynamically eliminated because of decreasing coherences (and so far vanishing correlations between populations at different energy levels).
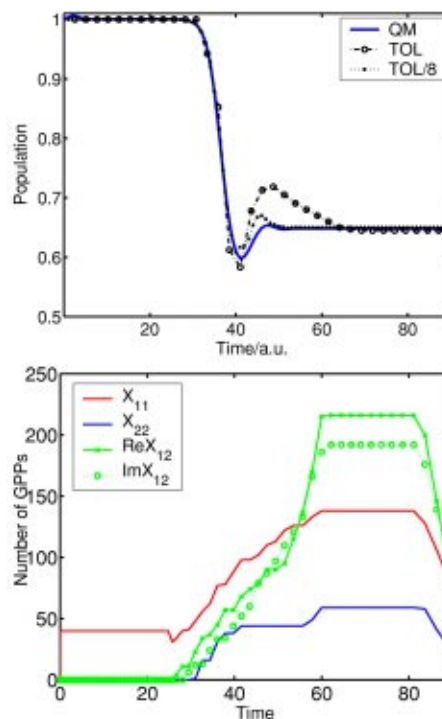

FIG. 2. (Top) Population of upper adiabatic state as function of time for *single crossing* potential. Solid line represents almost exact solution produced with the help of grid-based split-operator approach to corresponding Schrödinger equation. Two other lines show adaptive GPP solutions for two different tolerances ($\epsilon = \sqrt{m/M} = 0.01$; TOL = TOL$_x$ + TOL$_t$ = 1). (Bottom) Number of GPPs in representation of different matrix elements as function of time.

2. Double crossing

As it was shown in Ref. 60, the potential involving two consequent *avoided crossings* is the more demanding test for a numerical method. This is due to the importance of the correct description of interference effects. As we have already seen, appropriate transport of coherence plays a decisive role in propagation. Moreover, oscillatory behavior of the solution makes it difficult to represent a complex spatio-temporal structure of densities in terms of conventional particle sets. During the passage through the crossing region the maximal numerically feasible number of GPPs (1000) had been reached and the correlation between populations at different energy levels is not vanishing after the second crossing up to the end of integration. In general, as it was already demonstrated for the case of the classical Liouville equation,[55] the computational cost of the method is increasing whenever the geometric complexity of the solutions is growing with propagation time. Nevertheless, as it follows from Fig. 3, even for the *closed dynamical system* presented here there is a convergence of the implicit adaptive scheme towards the exact solution for the considered integration times. Due to the adaptivity, the method is able to reliably represent sophisticated spatio-temporal details of the dynamics under consideration.
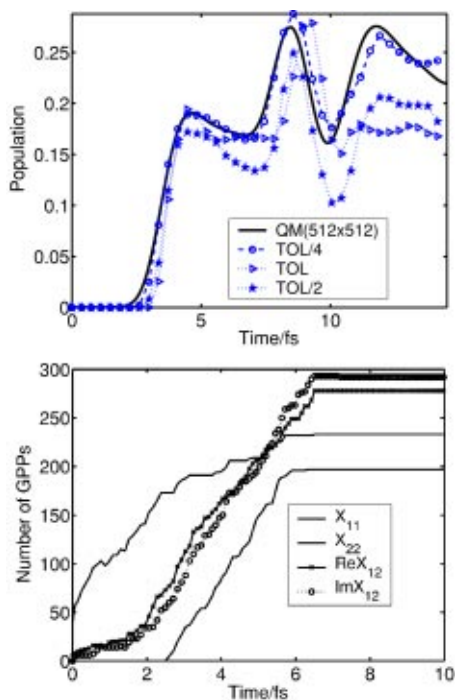
FIG. 3. (Top) Population of upper adiabatic state as function of time for the *dual crossing* potential. As in the case of the single crossing, the solid line represents the almost exact solution produced with the help of a grid-based split-operator approach to the corresponding Schrödinger equation. Three other lines show adaptive GPP solutions for three different tolerances ($\epsilon = \sqrt{m/M} = 0.01$; TOL$=1$). (Bottom) Number of GPP's in representation of different matrix elements as function of time.

B. Multidimensional examples

1. Pure quantum dynamics

In order to test the performance of the method in multidimensional cases we will first apply TRAIL to a coupled two-level system, with diabatic potential of the form

$$V(R) = \begin{pmatrix} V_{11}(R) & c \\ c & V_{22}(R) \end{pmatrix}, \tag{33}$$

where $V_{11}(R) = R_1^2 + R_2^2 + R_3^2$, $V_{22}(R) = V_{11} + E_0$ are three-dimensional harmonic oscillators and c is a constant coupling. Because the diabatic PESs are parallel, the exact population dynamics of such a system is given by a well-known Rabi formula.[71]

Figure 4 shows the population dynamics of the system as predicted from the diabatic variant of the TRAIL-scheme for two different global tolerances compared with analytically known result from the Rabi formula. The initial ground state density is represented by a single GPP and a set of Dirac-functions (being stochastically sampled according to the ground state distribution function). While the classical component of the QCLE-dynamics in this case is described simply by the Heller's formulas and can thus be exactly integrated by the predictor part of the TRAIL, the nonadiabatic exchange can only be reproduced in the corrector part of the scheme with the help of the adaptive creation/annihilation of the GPPs. Numerical solutions are converging towards the analytically known one with the reduction of the global tolerance.
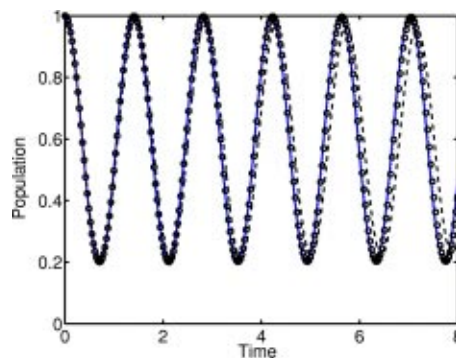

FIG. 4. Population of the lower diabatic state as a function of time for $\epsilon = 0.05$, $E_0 = 0.1$, $c = 0.1$. The solid line represents the analytically known solution. Two other lines show adaptive GPP solutions for two different tolerances: TOL$=0.02$ (dashed) and TOL$=0.01$ (circles).

The phase-space density in the analytical case is represented by four Gaussian densities: one for each of the diagonal elements of a density matrix, one for real and one for imaginary part of the off-diagonal element. Figure 5 (top) shows the adaptive time steps generated by TRAIL. As it can be seen, time steps get minimal values at the points where the population transfer curve achieves its extremal values. Adaptive phase-space discretization of the TRAIL-algorithm represents these perfectly well by choosing one GPP per density independently of the tolerance [see Fig. 5 (bottom)]. The minima of the curves (by 3 GPPs) are located where the
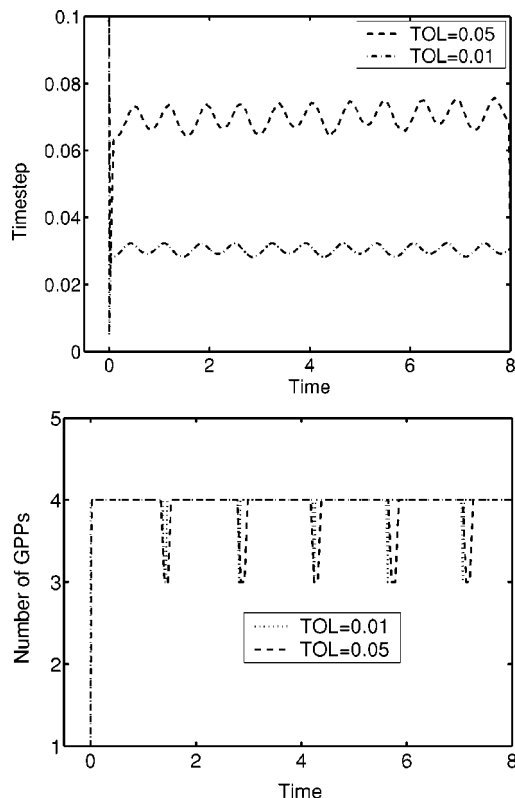

FIG. 5. Top: Time steps generated with TRAIL as functions of time for $\epsilon = 0.05$, $E_0 = 0.1$, $c = 0.1$ for two different tolerances: TOL$=0.02$ (dashed) and TOL$=0.01$ (dot-dashed). Bottom: Number of GPPs needed to afford the tolerances TOL$=0.02$ (dashed) and TOL$=0.01$ (dotted).
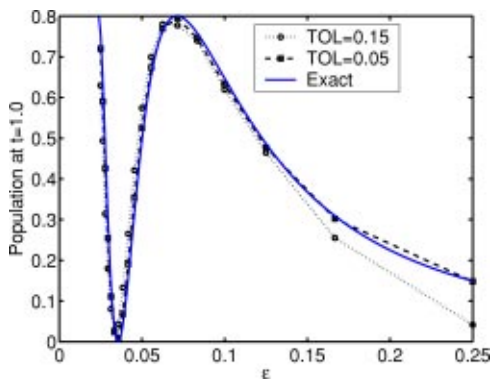
FIG. 6. Population of the upper harmonic oscillator at the time $t = 1.0$ as the function of ϵ.

population is concentrated almost only in the lower diabatic state, so the GPP in the upper state can be adaptively cancelled.

Figure 6 shows the values of the population of the upper harmonic oscillator at a fixed time $t = 1$ for different values of the smallness parameter $\epsilon = \sqrt{m/M}$. For decreasing ϵ the frequency of Rabi-oscillations increases which leads to a reduction of the adaptively chosen time steps. In this case the error is dominated by the nonadiabatic term of the QCLE, whereas for increasing values of ϵ the classical transport part will play a major role in accumulation of the error. As we can see TRAIL can reliably simulate both scenarios.

2. Quantum-classical dynamics: Conical intersection example

As a more demanding test for a QCLE-based implementation of the adaptive strategy we choose the two-state example of three-dimensional harmonic oscillators coupled linearly with the diabatic potential energy matrix of the form,

$$V(R) = \begin{pmatrix} V_{11}(R) & c(R) \\ c(R) & V_{22}(R) \end{pmatrix}, \tag{34}$$

where $V_{11}(R) = a(R_1^2 + R_2^2 + R_3^2) + aR_1$, $V_{22}(R) = a(R_1^2 + R_2^2 + R_3^2) - aR_1$ and $c(R) = bR_2$. This is a typical Hamiltonian for vibronic dynamics and spectroscopy.[1,2] This model can, for example, describe the photoexcitation process in Floquet representation[75] with continuous light and a dipole moment in linear approximation. In adiabatic representation two potential energy surfaces exhibit a *conical intersection* at $R = (0;0;0)$ which leads to numerical problems with conventional particle methods. The diabatic representation, in contrast, is more favorable in this respect. However, the practical *stochastic* implementation in the form of conventional *surface-hopping* particle methods seems to be more demanding in the diabatic case where the coupling (off-diagonal element of V) is typically not localized in space and time (in adiabatic case nonadiabatic effects occur only in the vicinity of the *crossing* of two potentials).

Figure 7 demonstrates the application of a diabatic variant of the TRAIL-method with *fixed maximal number* of allowed GPPs. This means that the space-discretization error is used to minimize the global tolerance with the number of GPPs kept constant. We start with Glauber state density of
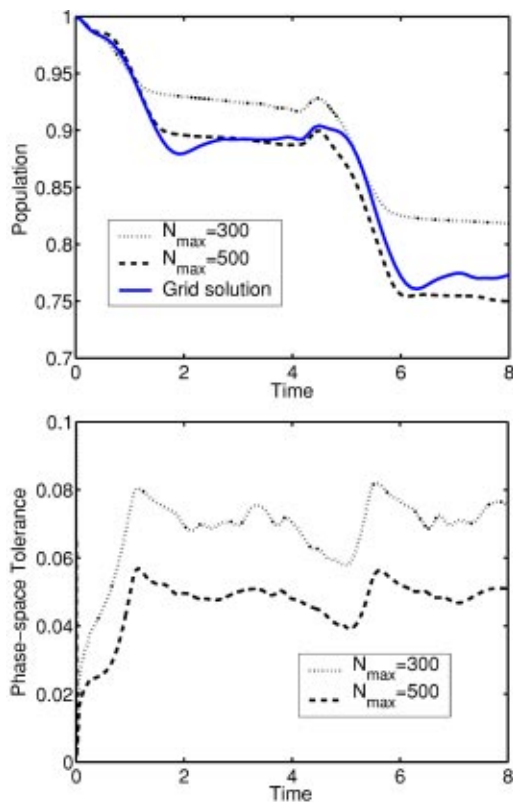

FIG. 7. (Top) Population of the left diabatic state as a function of time for $P_0 = (-0.5; 0; 0)$, $a = 1$, $b = 0.3$, $\epsilon = 0.1$. The solid line represents the grid-based solution. Two other lines show adaptive GPP solutions for two different maximally allowed numbers of GPPs: $N = 300$ (dotted) and $N = 500$ (dashed). Bottom: Phase-space tolerance as function of time for different numbers of maximally allowed GPPs.

the right diabatic state with momentum $P_0 = (-0.5; 0; 0)$, i.e., in the direction of the conical intersection. The curves show the population transfer during two passages of the density through the crossing region for two different numbers of maximally allowed GPPs. The curves produced by the TRAIL-approach are converging towards the grid-based solution (on a $64 \times 64 \times 64$ grid, derived with the help of the split-operator method) with increasing numbers of GPPs through the overall reduction of resulting global tolerance.

V. CONCLUSION

We presented a fully adaptive strategy for numerical simulation of nonadiabatic effects in molecular dynamics. This concept provides a possibility of controlling both space and time discretization errors and allows for a formulation of the particle method based on global tolerance criteria. A local error indicator is employed for creating new particles where needed, and the subcondition number of the influence matrix is exploited for removing particles which are no longer necessary for representing the distribution with a given global tolerance. In particular, this method is capable to treat nonadiabatic effects around conical intersections of PESs. Its performance is demonstrated for a spin-boson model in different dimensionality.

As it was shown for the one-dimensional numerical examples, the performance of the TRAIL-scheme with a *fixed*

global tolerance depends on the geometric complexity of solutions. In the case of the *double crossing* the actual phase-space densities and coherences acquire complex oscillatory structures which are expensive to resolve with small tolerances. Hence, a reliable representation of complex structures requires a large number of Gaussian particles. This problem can become crucial in multidimensional applications. As was shown for a conical intersection case in three dimensions, a computationally feasible alternative is the TRAIL-scheme with a *fixed maximally allowed number of GPPs*, which are optimally situated in phase-space according to the minimization of the global tolerance. In cases where phase-space structures are not too complex and can be represented with a moderate number of GPPs, the TRAIL-scheme allows for highly accurate integration of quantum-classical dynamics even for multidimensional systems.

ACKNOWLEDGMENTS

[1] W. Domcke and G. Stock, Adv. Chem. Phys. **100**, 1 (1997).
[2] D. R. Y. W. Domcke and H. Kppel, *Conical Intersections* (World Scientific, Singapore, 2003).
[3] J. Michl and V. Bonačić-Koutecký, *Electronic Aspects of Organic Photochemistry* (Wiley, New York, 1990).
[4] E. P. Wigner, Phys. Rev. **40**, 749 (1932).
[5] R. Kapral and G. Ciccotti, J. Chem. Phys. **110**, 8919 (1999).
[6] C. Schütte, Konrad-Zuse-Center, Preprint SC-99-10 (1999), available through http://www.zib.de/bib
[7] S. Nielsen, R. Kapral, and G. Ciccotti, J. Chem. Phys. **112**, 6543 (2000).
[8] R. Kapral, J. Phys. Chem. A **105**, 2885 (2001).
[9] M. Santer, U. Manthe, and G. Stock, J. Chem. Phys. **114**, 2001 (2001).
[10] D. McKernan, G. Ciccotti, and R. Kapral, J. Chem. Phys. **116**, 2346 (2002).
[11] C. Zenger, Notes Numer. Fluid Mech. **31**, 241 (1991).
[12] M. Griebel and G. Zumbusch, ''Adaptive sparse grids for hyperbolic conservation laws,'' in *Hyperbolic Problems: Theory, Numerics, Applications, in Proceedings of the 7th International Conference*, Zürich, Switzerland, February 1998, Vol. 1 in Int. Ser. Numer. Math. 129, edited by M. Fey (Basel, Birkhäuser, 1999), pp. 411–422.
[13] H. Neunzert, A. Klar, and J. Struckmeier, ''Particle Methods: Theory and Applications,'' in ICIAM 95: Proceedings of the Third International Congress on Industrial and Applied Mathematics held in Hamburg, Germany, edited by K. Kirchgaessner, 1995.
[14] *Meshfree Methods for Partial Differential Equations. Lecture Notes in Computational Science and Engineering 26*, edited by M. Griebel and M. A. Schweitzer (Springer, New York, 2002).
[15] E. J. Heller, J. Chem. Phys. **68**, 2066 (1978).
[16] E. J. Heller, Acc. Chem. Res. **14**, 368 (1981).
[17] S.-I. Sawada and R. Heather, J. Chem. Phys. **83**, 3009 (1985).
[18] S.-I. Sawada and H. Metiu, J. Chem. Phys. **84**, 6293 (1986).
[19] P. Bala, P. Grochowski, B. Lesyng, and J. A. McCammon, J. Phys. Chem. **100**, 2535 (1996).
[20] F. A. Bornemann, P. Nettesheim, and C. Schütte, J. Chem. Phys. **105**, 1074 (1996).
[21] P. Nettesheim, F. A. Bornemann, B. Schmidt, and C. Schütte, Chem. Phys. Lett. **256**, 581 (1996).
[22] P. Nettesheim, Konrad-Zuse-Center, Preprint No. SC-98-37 (1998), available through http://www.zib.de/bib
[23] J.-Y. Fang and S. Hammes-Schiffer, J. Chem. Phys. **110**, 11166 (1999).
[24] M. Hochbruck and C. Lubich, Biomaterials **39**, 620 (1999).
[25] M. Hochbruck and C. Lubich, SIAM (Soc. Ind. Appl. Math.) J. Numer. Anal. **41**, 945 (2003).
[26] T. Jahnke and C. Lubich, Numer. Math. **94**, 289 (2003).
[27] P. Grochowski and B. Lesyng, J. Chem. Phys. **119**, 11541 (2003).
[28] J. C. Tully, J. Chem. Phys. **93**, 1061 (1990).
[29] D. F. Coker, in *Computer Simulation in Chemical Physics*, edited by M. P. Allen and D. J. Tildesley (Kluwer, Netherlands, 1993), pp. 315–377.
[30] J. C. Tully, in *Classical and Quantum Dynamics in Condensed Phase Simulations*, edited by B. J. Berne, G. Ciccotti, and D. F. Coker (World Scientific, Singapore, 1998), pp. 700–720.
[31] L. Seidner and W. Domcke, Chem. Phys. **186**, 27 (1994).
[32] T. Terashima, M. Shiga, and S. Okazaki, J. Chem. Phys. **114**, 5663 (2001).
[33] S. R. Billeter, S. P. Webb, T. Iordanov, P. K. Agarwal, and S. Hammes-Schiffer, J. Chem. Phys. **114**, 6925 (2001).
[34] D. Zahn and J. Brickmann, Phys. Chem. Chem. Phys. **3**, 848 (2001).
[35] M. Wang and J. Z. H. Zhang, J. Chem. Phys. **119**, 11152 (2003).
[36] N. Doltsinis and D. Marx, Phys. Rev. Lett. **88**, 166402 (2002).
[37] E. J. Heller, J. Chem. Phys. **62**, 1544 (1975).
[38] R. C. Brown and E. J. Heller, J. Chem. Phys. **75**, 186 (1981).
[39] G. Drolshagen and E. J. Heller, J. Chem. Phys. **75**, 186 (1981).
[40] G. Drolshagen and E. J. Heller, J. Chem. Phys. **75**, 186 (1981).
[41] T. J. Martinez and M. Ben-Nun, J. Chem. Phys. **104**, 2847 (1996).
[42] T. Martinez and M. Ben-Nun, J. Phys. Chem. **100**, 7884 (1996).
[43] M. Ben-Nun and T. J. Martinez, J. Chem. Phys. **108**, 7244 (1998).
[44] C.-C. Wan and J. Schofield, J. Chem. Phys. **112**, 4447 (1999).
[45] C.-C. Wan and J. Schofield, J. Chem. Phys. **113**, 7047 (2000).
[46] C.-C. Wan and J. Schofield, J. Chem. Phys. **116**, 494 (2002).
[47] R. Walkup, J. Chem. Phys. **95**, 6440 (1991).
[48] O. Prezhdo and V. V. Kisil, Phys. Rev. A **56**, 162 (1997).
[49] V. Buch, J. Chem. Phys. **117**, 4738 (2002).
[50] I. Burghardt, M. Nest, and G. Worth, J. Chem. Phys. **119**, 5364 (2003).
[51] S. Garashchuk and V. Rassolov, J. Chem. Phys. **118**, 2482 (2003).
[52] G. Billing, J. Chem. Phys. **110**, 5526 (1999).
[53] G. Billing, J. Chem. Phys. **114**, 6641 (2001).
[54] P. Deuflhard, J. Lang, and U. Nowak, ''Recent progress in dynamical process simulation,'' in *Progress in Industrial Mathematics, in Proceedings of the 8th Conference of the European Consortium for Mathematics in Industry*, edited by H. Neunzert (Wiley and Teubner, New York, 1996, pp. 122–137.
[55] I. Horenko and M. Weiser, J. Comput. Chem. **24**, 1921 (2003).
[56] D. R. Yarkony, Rev. Mod. Phys. **68**, 985 (1996).
[57] H. Koeppel, J. Gronki, and S. Mahapatra, J. Chem. Phys. **115**, 2377 (2001).
[58] S. Hammes-Schiffer and J. C. Tully, J. Phys. Chem. **99**, 5793 (1995).
[59] M. Vener, O. Kühn, and J. Sauer, J. Chem. Phys. **114**, 240 (2001).
[60] I. Horenko, C. Salzmann, B. Schmidt, and C. Schütte, J. Chem. Phys. **117**, 11075 (2002).
[61] S. Nielsen, R. Kapral, and G. Ciccotti, J. Chem. Phys. **115**, 5805 (2001).
[62] M. Hillery, R. F. O'Connell, M. O. Scully, and E. P. Wigner, Phys. Rep. **106**, 121 (1984).
[63] I. Horenko, B. Schmidt, and C. Schütte, J. Chem. Phys. **117**, 4643 (2002).
[64] F. Bornemann, IMPACT Comput. Sci. Eng. **2**, 279 (1990).
[65] P. Deuflhard and W. Sautter, Lin. Algebra Appl. **29**, 91 (1980).
[66] A. Iske and J. Levesley, Technical Report, University of Leicester **17** (2002).
[67] R. Schaback and H. Wendland, Numer. Algorithms **24**, 239 (2000).
[68] R. S. Y. C. Hon and X. Zhoud (preprint, 2001).
[69] P. Businger and G. H. Golub, Numer. Math. **7**, 269 (1965).
[70] J. Ma, D. Hsu, and J. E. Straub, J. Chem. Phys. **99**, 4024 (1993).
[71] S. Mukamel, *Principles of Nonlinear Optical Spectroscopy* (Oxford University Press, New York, 1995).
[72] W. P. Schleich, *Quantum Optics in Phase Space* (Wiley-VCH, Berlin, 2001).
[73] P. Deuflhard and V. Apostolescu, ''An underrelaxed Gauss–Newton method for equality constrained nonlinear least squares problems,'' in Optimization Techniques, Proceedings of the 8th IFIP Conference, Würzburg, 1977, Springer Lecture Notes Control Inf. Sci. 7, edited by J. Stoer, 1978, pp. 22–32.
[74] R. Kosloff, Annu. Rev. Phys. Chem. **45**, 145 (1994).
[75] I. Horenko, B. Schmidt, and C. Schütte, J. Chem. Phys. **115**, 5733 (2001).